AD-A176 354 RELATIVISTIC ELECTRON BEAM PROPAGATION IN THE ION FOCUSING REGIME(U) NAVAL SURFACE WEAPONS CENTER SILVER SPRING MD J R SMITH ET AL 01 AUG 86 NSWC/TR-86-274 1/1

UNCLASSIFIED F/G 20/7 NL

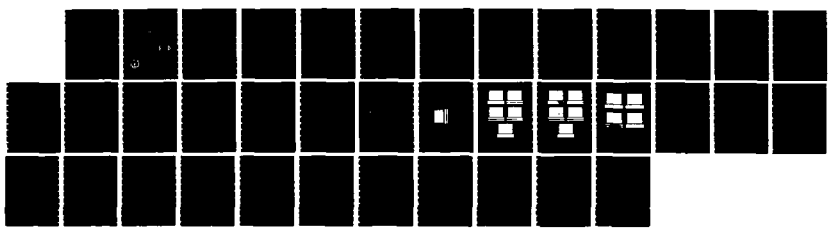

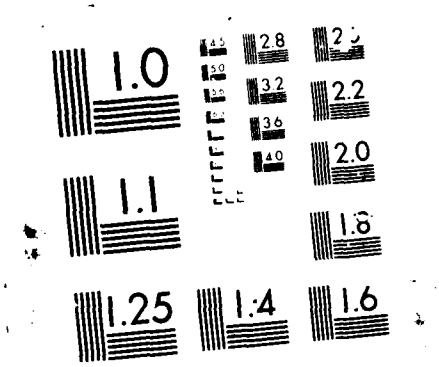
1.0
1.1
1.25
2.8
3.2
3.6
4.0
2.2
2.0
1.8
1.4
1.6

NSWC TR 86-274

AD-A176 354

RELATIVISTIC ELECTRON BEAM PROPAGATION IN THE ION FOCUSING REGIME

BY J. R. SMITH R. F. SCHNEIDER H. S. UHM W. NAMKUNG M. RHEE

RESEARCH AND TECHNOLOGY DEPARTMENT

1 AUGUST 1986

DTIC
ELECTE
FEB 0 3 1987
S D
D

Approved for public release; distribution is unlimited.

NAVAL SURFACE WEAPONS CENTER

Dahlgren, Virginia 22448-5000 • Silver Spring, Maryland 20903-5000

DTIC FILE COPY

87 2 2 002

UNCLASSIFIED

SECURITY CLASSIFICATION OF THIS PAGE

REPORT DOCUMENTATION PAGE

1a. REPORT SECURITY CLASSIFICATION Unclassified	1b. RESTRICTIVE MARKINGS
2a. SECURITY CLASSIFICATION AUTHORITY	3. DISTRIBUTION/AVAILABILITY OF REPORT Approved for public release; distribution unlimited.
2b. DECLASSIFICATION/DOWNGRADING SCHEDULE	
4. PERFORMING ORGANIZATION REPORT NUMBER(S) NSWC TR 86-274	5. MONITORING ORGANIZATION REPORT NUMBER(S)
6a. NAME OF PERFORMING ORGANIZATION Naval Surface Weapons Center 6b. OFFICE SYMBOL (If applicable) R41	7a. NAME OF MONITORING ORGANIZATION
6c. ADDRESS (City, State, and ZIP Code) 10901 New Hampshire Avenue Silver Spring, Maryland 20903-5000	7b. ADDRESS (City, State, and ZIP Code)
8a. NAME OF FUNDING/SPONSORING ORGANIZATION I. R. Fund Naval Surface Weapons Center 8b. OFFICE SYMBOL (If applicable) R04	9. PROCUREMENT INSTRUMENT IDENTIFICATION NUMBER
8c. ADDRESS (City, State, and ZIP Code) 10901 New Hampshire Avenue Silver Spring, Maryland 20903-5000	10. SOURCE OF FUNDING NUMBERS PROGRAM ELEMENT NO. / PROJECT NO / TASK NO / WORK UNIT ACCESSION NO.

11. TITLE (Include Security Classification)

Relativistic Electron Beam Propagation in the Ion Focusing Regime

12. PERSONAL AUTHOR(S) Smith, J. R., Schneider, R. F., Uhm, H. S., Namkung, W., Rhee, M.

13a. TYPE OF REPORT	13b. TIME COVERED	14. DATE OF REPORT (Year, Month, Day)	15. PAGE COUNT
Final	FROM 6/85 TO 6/86	1986, August, 1	38

16. SUPPLEMENTARY NOTATION

17. COSATI CODES			18. SUBJECT TERMS (Continue on reverse if necessary and identify by block number)
FIELD	GROUP	SUB-GROUP	
20	09		Electron Beam, Ion Focused Regime.

19. ABSTRACT (Continue on reverse if necessary and identify by block number)

This report presents observations on propagation of a mildly relativistic electron beam ($\gamma = 2.4$) in several different gases (air, He, N_2 and Ar) at low pressure (10-320 mTorr). At such low pressures, and with beam currents of several kiloamperes, beam induced ionization may result in self-focusing of an electron beam. Beams propagating under this condition are said to be in the ion focusing regime of propagation. The injected beam has an rms radius of 0.7 cm and a transverse temperature of 35 keV. Beam transport efficiency was measured for He, N_2 and Ar. A simple calculation was performed to determine the space charge neutralization fraction as a function of time. Using the results of this calculation, the charge transport efficiency is found and compared with the experimentally measured quantity.

20. DISTRIBUTION/AVAILABILITY OF ABSTRACT	21. ABSTRACT SECURITY CLASSIFICATION
☒ UNCLASSIFIED/UNLIMITED ☐ SAME AS RPT ☐ DTIC USERS	UNCLASSIFIED
22a. NAME OF RESPONSIBLE INDIVIDUAL J. R. Smith	22b. TELEPHONE (Include Area Code) (202)394-2597
	22c. OFFICE SYMBOL R41

DD FORM 1473, 84 MAR 83 APR edition may be used until exhausted. All other editions are obsolete.

SECURITY CLASSIFICATION OF THIS PAGE

★U.S. Government Printing Office: 1985—635-012

0102-LF-014-6602

UNCLASSIFIED

FOREWORD

This report presents observations on propagation of a mildly relativistic electron beam (γ = 2.4) in several different gases (air, He, N_2, and Ar) at low pressure (10-320 mTorr). At such low pressures, and with beam currents of several kiloamperes, beam induced ionization may result in self-focusing of an electron beam. Beams propagating under this condition are said to be in the ion focusing regime of propagation. The injected beam has an rms radius of 0.7 cm and a transverse temperature of 35 keV. Beam transport efficiency was measured for He, N_2 and Ar. A simple calculation was performed to determine the space charge neutralization fraction as a function of time. Using the results of this calculation, the charge transport efficiency is found and compared with the experimentally measured quantity. We gratefully acknowledge helpful discussions with Dr. Khanh T. Nguyen and technical assistance provided by Herman I. Cordova and John F. Wood. This work was supported by the Independent Research Fund at NSWC.

Approved by:

Carl W. Larson

CARL W. LARSON, Head
Radiation Division

Accesion For
NTIS CRA&I ☑
DTIC TAB ☐
Unannounced ☐
Justification .....
By .....
Distribution/
Availability Codes
Dist | Avail and/or Special
A-1

CONTENTS

ILLUSTRATIONS

TABLES

CHAPTER 1

INTRODUCTION

A propagation window exists for intense relativistic electron beam injection into a low pressure (sub-Torr) neutral gas. Previously such propagation has been experimentally observed.[1-9] The results of any particular experiment are highly parameter dependent; beam current, pulse duration, transverse beam temperature, gas species, etc. may determine propagation characteristics. In this work we have measured several key quantities which affect propagation and compared them with a simple model to explain the propagation results for different gases and pressures. Two conditions necessary for propagation are: (1) the beam current must be below the space charge limiting current and (2) the beam electrons must see radial force balance.

The space charge limiting current is determined from the criterion that the kinetic energy of an electron at the beam's center be less than its potential energy. Otherwise the beam is "stopped" axially and a potential well is created. The expression for space charge limiting current for a solid beam propagating in an infinite cylindrical conductor is given by[10]

$$I_\ell = \frac{mc^3}{e} \frac{(\gamma^{2/3}-1)^{3/2}}{[1+2\ln(R/r)]\,(1-f_e)} \qquad (1)$$

where γ is the usual relativistic factor, m is electron mass, c is the speed of light in vacuum, e is the electron charge, R is the conductor radius, and r is the beam radius. Here f_e is the space charge neutralization fraction where $f_e \equiv n_i/n_b$ $(0<f_e<1)$; n_b is the electron beam density and n_i is the density of a charge neutralizing ion background. In order to satisfy propagation condition (1) which was stated above, the beam current must be less than I_ℓ.

The condition for equilibrium for a beam with a Bennett density profile may be expressed as[11]

$$f_e = \frac{1}{\gamma^2} + \frac{2T_\perp}{\nu mc^2} \qquad (2)$$

where ν is Budker's parameter and $T_\perp$ is the beam's transverse temperature. The assumptions made here are: no beam rotation and gas pressure low enough so there is no current neutralization. If $f_e > 1/\gamma^2 + 2T_\perp/\nu mc^2$ propagation still occurs, but the beam electrons oscillate within the beam envelope. This oscillation has been previously analyzed elsewhere.[12,13]

Both of the propagation conditions critically depend on f_e (i.e. the degree of charge neutralization). Charge neutralization may be created by the electron beam itself as an alternative to employing an external source of ionization. The background gas is ionized as the relativistic electron beam is injected, therefore creating a plasma. Plasma electrons are radially ejected by the beam's high electric field leaving a channel of positive charge. This ion channel reduces the beam's space charge force such that $f_e > 1/\gamma^2 + 2T_\perp/\gamma mc^2$, thereby permitting a focused beam. This is called propagation in the ion focusing regime (IFR). During their ejection the plasma electrons must not create significant additional secondary electrons (i.e. the mean free path for ionization by secondary electrons must be much less than the beam radius). This requirement was used by Briggs and Yu to determine an upper bound on pressure for which IFR propagation can occur.[14] This critical pressure is given as

$$p_c \sim \frac{I_B}{a_0} \, s \qquad (3)$$

where I_B is the beam current, a_0 is the fully-pinched beam radius, and s is a scale factor which depends on the model used for ionization cross section as a function of energy. The scale factor is normalized to nitrogen gas and has the following values for some common gases: SF_6 - 0.27, argon - 0.9, nitrogen - 1, neon - 2.0, helium - 5.9. Therefore, for the beam used in this work the upper limit on pressure for IFR propagation is 2.4 Torr for helium, 0.4 Torr for nitrogen or air, and 0.4 Torr for argon.

This TR is organized in the following manner. In Chapter 2 a brief description of the accelerator is given. Chapter 3 contains current transport measurements and Chapter 4 describes emittance measurements on the propagating electron beam. A simple model for beam propagation in low pressure gas is developed in Chapter 5 and is used to calculate the efficiency of charge transport. This model assumes idealized conditions and gives an upper limit on transport efficiency. The measured charge transport is then compared with calculated results. Chapter 6 is a summary. The work presented here augments previous research on low pressure propagation in its emphasis on beam temperature as an influence on beam transport. We have also included pulse rise time effects which are not generally included in other investigations.

CHAPTER 2

TRANSBEAM ACCELERATOR

A brief discussion of the accelerator used for this work is given since it has several features not common to other accelerators with similar specifications. The Transbeam accelerator at NSWC uses a high-voltage, air-core pulse transformer to charge a water-filled coaxial transmission line to produce a 100 ns duration electron beam. Transformers have some advantages over the Marx generators that are generally used in accelerators, such as (1) they allow for a more compact design since an oil filled tank is not necessary, and (2) they greatly reduce the number of spark gaps needed and therefore require less maintenance. Figure 1 is a schematic of the accelerator with representative machine diagnostic traces. The high voltage transformer was designed similar to that of Rohwein[15] and has a 3 MV secondary voltage for a 100 kV primary voltage. Resonant charging of the transmission line (i.e. the resonant frequency of the transformer primary circuit is matched to the resonant frequency of the transformer secondary circuit, $L_pC_p = L_sC_s$) allows maximum energy transfer efficiency. Single resonance charging, where the maximum output voltage is attained on the peak of the first half cycle, requires a transformer circuit with coefficient of coupling near unity which is difficult to achieve in a high-voltage, high-gain transformer. Dual resonance charging, where the maximum output voltage is attained on the peak of the second half cycle, requires a coupling coefficient[16] of 0.6 which is more easily obtained in transformer construction. This is the method of charging used on Transbeam. The output switch gas pressure is adjusted so that the transmission line discharges on the peak of the second half cycle as shown in Figure 1. Note that the diode voltage is one half of the transmission line charging voltage for a matched diode impedance. A short isolation section inserted between the transmission line and the diode promotes suppression of diode prepulse. In the work described here the voltage applied to the transformer primary was 50 kV, which resulted in a peak diode voltage of 700 kV.

The diode consisted of a 7.5 cm diameter planar carbon cathode and a 0.6 mil titanium anode foil. The gap spacing was 15 mm. Diode voltage and current waveforms are shown in Figure 1. Using stopping power calculations for 700 keV electrons, less than 2% of an electron's kinetic energy was lost in the anode foil. A carbon plate with a 2 cm diameter aperture was placed immediately downstream of the anode foil. This plate limited the beam current injected into the drift tube to about 4 kA.

CHAPTER 3

BEAM TRANSPORT MEASUREMENTS

The efficiency of beam transport was measured using the set-up depicted in Figure 2. The beam was injected into a 10 cm diameter conducting tube. A Rogowski coil was positioned at the drift tube entrance and measures net current. The vacuum Faraday cup was located 1 m downstream of the anode foil. It consists of a 7.5 cm diameter carbon beam stop connected to an 0.005 Ω current viewing resistor which has a 2 ns risetime. A 0.6 mil titanium foil provides the interface between the gas-filled propagation tube and the evacuated Faraday cup. Both the Rogowski coil and Faraday cup were connected to a dual-beam oscilloscope and typical traces for a 40 mTorr argon shot are given in Figure 2. The Rogowski signal is integrated with a passive RC integrator. The oscilloscope and diagnostic cables were adjusted so that two synchronous signals also appear synchronous on the oscillographs. In order to permit open shutter photography a section of the propagation tube consisted of a pyrex tube lined inside with a perforated stainless steel sheet. Before each shot the tube was evacuated to 1×10^{-5} Torr. It was then static filled with either He, N_2 or Ar at pressures of 10, 20, 40, 80 or 160 mTorr. Impurities from outgassing contributed about 2 mTorr to the total pressure of each shot. Sample results for nitrogen gas at different pressures are given in Figure 3. The upper oscilloscope trace is the transmitted beam current as measured by the Faraday cup (2kA/div). The lower trace is the net current measured with a Rogowski coil immediately downstream of the anode plate (3 kA/div). Open shutter photographs are shown for each shot. At 10 mTorr no beam was propagated. At 20 mTorr the latter half of the beam propagated. The total beam was propagated for the pressures of 80 and 160 mTorr. For the lower pressures the beam is significantly eroded. The integrated Rogowski coil signals show appreciable trailing plasma current for all but the 10 mTorr shot. All open shutter photographs were taken at the same exposure settings therefore light intensity at different pressures may be compared. Data for the argon shots (Figure 4) closely agree with the nitrogen shots. Helium propagation (Figure 5) was different in that no propagation occurred at 10, 20 or 40 mTorr; only slight propagation at 80 mTorr; and at 160 mTorr only the latter half of the beam propagated. Propagation results for all three gases are summarized in Figure 6 where the peak Faraday cup current is plotted as a function of gas pressure.

CHAPTER 4

EMITTANCE MEASUREMENTS CHARACTERIZING BEAM PROPAGATION IN AIR

A detailed analysis of beam propagation in air was performed as follows. The beam was injected into either a 10 cm diameter stainless steel drift tube or a 10 cm acrylic tube lined with copper screen wire which permitted photographic diagnostics. Tube length was varied in order to observe propagation behavior as a function of axial distance. The experiment was performed in vacuum with the drift tube at 0.01 mTorr and with air admitted at pressures of 20, 40, 80, 160, and 320 mTorr. By comparison of open shutter photographs and Faraday cup signals, propagation in air closely resembled propagation in nitrogen. Beam emittance and radius were measured as a function of axial position (z). An emittance mask was used which consisted of a series of tantalum bars, each with cross sectional dimensions of 0.4 x 5.0 mm. The bars were separated with an 0.5 mm slit width. An 0.05 mm thick radiachromic film detector[17] was placed 4.3 mm downstream from the mask. After exposure to a single shot the film was scanned with a microdensitometer using a resolution of 0.02 mm. Since the film was exposed at rather high levels, it was scanned with light of wavelength 510 nm where the film response is linear at high exposure. Results for scans at different axial positions and pressures are shown in Figure 7.

The following is a brief description of the emittance theory used to analyze beam emittance. A complete derivation of this theory is given in Reference 18. Two assumptions made are: (1) an axisymmetric beam, and (2) a local thermal distribution (Maxwellian). Using these assumptions the distribution function in transverse trace space may be written as

$$f_4(x,y,x',y') = g(\sqrt{x^2+y^2}) \exp\{-[(x' - \bar{x}')^2 + (y' - \bar{y}')^2]/2s^2(x,y)\} \quad (4)$$

where $x' = dx/dz$ and $y' = dy/dz$ are the slopes of the particle trajectory, $g(\sqrt{x^2+y^2})$ is the spatial dependence of the distribution function, s is the rms value of the particle slopes at a point (x,y), and $\bar{x}'$ and $\bar{y}'$ are the mean values of particle slopes at a point (x,y). The rms emittance is given by

$$\varepsilon_{rms} = 4[\langle x^2\rangle \langle x'^2\rangle - \langle xx'\rangle^2]^{1/2} \quad (5)$$

where < > denotes the average over the four dimensional trace space distribution function. This treatment relates to our work in the following manner. We take the slits of the emittance meter as being aligned parallel to the y axis. The radiachromic film which is placed downstream of the slits is scanned along the x axis. Therefore the beam is first sampled directly through the slits of the emittance meter, and then through the pinhole of the microdensitometer (via the radiachromic film image). By analysis of the microdensitometer scan we can determine $g(x,y=0)$, $s(x,y=0)$, and $\bar{x}'(x,y=0)$. Using the assumptions made, $f_4(x,y,x',y')$ is determined over all space, and the rms emittance is calculated numerically according to Eq. (5). Results are given in Figure 8, where the rms emittance characterizing the beam at injection (z = 3 cm, p = 0 mTorr) was 0.55 cm-rad which corresponds to a transverse temperature of 35 keV. We observed that this emittance value typically increased by a factor of 1.5 to 2 after a short propagation distance (10 cm). The measured beam emittance remained somewhat constant after this initial increase. The rms radii determined by $x_{rms} = [\langle x^2 \rangle]^{1/2}$ are summarized in Figure 9. The injected beam is characterized by a 0.7 cm radius. For comparison one notes that the beam is injected through an aperture with a 1 cm radius. As the beam propagates further downstream the rms radius varies from 1.2 to 1.5 times the radius of the injected beam. The data in Figure 9 as well as open shutter photographs reveal pinch points and oscillations in the beam envelope. This is caused by overcompensation of the beam's radial electric field by ions which results in the oscillatory electron motion.

CHAPTER 5

ANALYSIS

When beam electrons are used as the ion production mechanism for IFR propagation, the space charge neutralization fraction and space charge limiting current both vary in time. Therefore the first part of the pulse may not lie in a propagation regime while the latter part does. The beam pulse is taken to start at t=0. At some later time τ such that (1) $I_b < I_\ell$ and (2) $f_e > 1/\gamma^2 + 2T_\perp/\gamma mc^2$ the two conditions for propagation stated in Chapter 1 are met and the beam may propagate. A simple calculation which follows was used to approximate $f_e(t)$ and $I_\ell(t)$ for our beam parameters in order to find this time τ at which both conditions for propagation are met.

First an expression for the temporal dependence of f_e is derived. Ionization of a neutral gas may occur through several competing processes such as electron impact ionization, electron avalanche ionization, ion imapct ionization, or ion avalanche ionization.[19] As noted in Chapter 1, we are below the pressures where secondary plasma electrons can cause electron avalanche ionization upon their expulsion from the channel. Ion impact ionization is a factor when plasma ions are accelerated to high energies via the collective acceleration process. However, using CR-39 ion detector plates, no high energy ions were observed in any of the several shots where they were monitored. Ion avalanche ionization may be a factor and should be considered in a more extensive analysis, however its inclusion is beyond the scope of this work. Our treatment therefore includes only electron impact ionization involving the primary beam electrons. The expression for ion production rate may be given as

$$\frac{\partial n_i(r,t)}{\partial t} = n_b(r,t)\, n_n\, \sigma(t)\, \beta(t)\, c \qquad (6)$$

where n_i is the ion density, n_b is the beam density, n_n is the neutral gas density, and σ is the cross section for ionization by electron impact. The beam density is taken to have a Gaussian distribution and may be expressed in terms of the beam current as

$$n_b(r,t) = \frac{I_b(t)}{\pi a^2 ec\, \beta(t)}\, e^{-r^2/a^2} \qquad (7)$$

Equation (7) is inserted into Eq. (6) which is solved for $n_i(r,t)$. Then f_e may be written as

$$f_e(t) = \frac{n_n\ \beta(t)\ c}{I_b(t)} \int_{t_o}^{t} I_b(t')\ \sigma(t')\ dt' \ , \qquad (8)$$

where we have assumed that only singly charged ions are present. The functions appearing in Eq. (8) are determined as follows. Trapezoidal waveforms are used to approximate the actual measured beam current, $I_b(t)$, and voltage, $V(t)$. The pulse risetime and falltime are each 30 ns and the plateau duration is 80 ns. The plateau value of current (voltage) is 4 kA (600 kV). The functions $\gamma(t)$ and $\beta(t)$ are obtained from the trapezoidal function for $V(t)$. Since the voltage function has temporal dependence, the ionization cross section which depends on electron energy, is also time dependent. Reference 20 gives an empirical formula for electron impact ionization cross section for many commonly used gases. Their formula is the result of empirical measurements of the cross section for electron energies in the range from 0.1 to 2.7 MeV. Hence using the cross section formula of Reference 20 and the beam energy as a function of time, $\sigma(t)$is found. Finally Eq. (8) is solved numerically to find $f_e(t)$. Representative results are given in Figure 10. In all cases full charge neutralization (i.e. f_e=1) was achieved during the beam pulse. For nitrogen and argon at the higher pressures, full charge neutralization occurred very early in the beam pulse, during the pulse risetime. The space charge neutralization fraction increases linearly during the pulse plateau. The rate of increase in f_e is greater at the pulse falltime since the ion channel remains while the beam density dies away. The limiting current as a function of time, $I_\ell(t)$, is calculated by inserting Eq. (8) and $\gamma(t)$ into Eq. (1). For calculation of I_b the measured radius of the injected beam, 0.7 cm, was used.

The trapezoidal function for $I_b(t)$, which is an idealization but close approximation of our beam current, is compared with $I_\ell(t)$ in order to determine when condition (1) for propagation is met. (See Figure 11 for comparison of $I_b(t)$ and $I_\ell(t)$ for He and Ar at 20 and 160 mTorr.) With our particular experimental parameters, initially the injected beam current was always greater than the space charge limiting current. As f_e increases due to the IFR process, the beam current consequently falls below the space charge limiting current (the limiting current increases since $I_\ell \propto (1-f_e)^{-1}$). The rate of increase of f_e is greater for higher gas pressures and for gases with higher ionization cross sections, and therefore the time required to satisfy propagation condition (1) in these cases is less. Note that the ionization cross section for N_2 and Ar is an order of magnitude greater than that of He (@ 600 keV) so the time necessary to satisfy propagation condition (1) is less for the former two gases. The time required for the beam current to fall below the space charge limiting current under different parameters is summarized in Table 1.

The quantities needed to test condition (2) for propagation are determined as follows. The fractional charge neutralization, $f_e(t)$ is found as previously described. The functions $\gamma(t)$ and $\nu(t)$ are derived from the trapezoidal voltage and current waveforms. The transverse temperature, $T_\perp$, is approximated by a trapezoidal waveform. This waveform is taken to have a plateau of 35 keV which is the measured transverse temperature of the injected beam. The temporal

dependence of f_e and $(1/\gamma^2 + 2T_\perp/\gamma mc^2)$ are then compared in order to determine the time at which condition (2) is satisfied. (See Figure 12 for this comparison for He and Ar at 20 and 160 mTorr.) Initially, before sufficient ions are created, the beam experiences radial expansion. If the necessary quantity of ions are produced at some later time in the beam pulse, propagation condition (2) is satisfied. The time required for achieving condition (2) under different parameters is summarized in Table 2.

In all cases the time required to reach self-pinched equilibrium exceeded the time at which the beam current fell below the space charge limiting current, so for our beam parameters propagation condition (2) was the controlling factor. Therefore the time as listed in Table 2 indicates when both conditions for propagation are met, this time being defined as $t = \tau$. The portion of beam pulse which lies in the interval from 0 to τ does not propagate, while the latter portion in the interval from τ to 140 ns (i.e. the beam's terminus) may propagate. Thus using the results of Table 2, the percent of the total injected charge which propagates (under ideal conditions) was calculated.

The percent of injected charge which propagated (a distance of 1 m) was measured as follows. The transported beam charge was determined from the current pulse signal of the Faraday cup which was located 1 m downstream of the anode. On a separate shot the injected beam charge was found using the current pulse measured by the Rogowski coil located at the drift tube's entrance. For this shot the drift tube was evacuated to less than 1×10^{-5} Torr. In this case no plasma currents are present, therefore the net current can be regarded as the beam current. A comparison of the many shots in which injected charge was measured indicates no appreciable shot to shot variation. The ratio of transported/injected charge as measured is compared with that calculated in Figure 13.

Three explanations for the difference in the calculated and measured curves are given. First, note that the calculated value of $f_e(t)$ used to determine charge transport was derived assuming that the entire injected pulse ionizes the filling gas along the entire drift tube length. Actually $f_e(t)$ is an axially varying function since beam duration decreases as propagation distance increases. If the Faraday cup had been closer to the diode such that f_e had less axial variation over its propagation distance, we would expect more absolute agreement between the measured and calculated transported charge. Secondly, in the calculation of $f_e(t)$ we assume that plasma electrons are instantaneously ejected from the channel. As f_e approaches unity the radial electric fields are decreased and plasma electrons are not as readily expelled. Thirdly, at the higher nitrogen and argon pressure used in this work (i.e. 160 mTorr) we are approaching the critical pressure for IFR propagation[14] and plasma electrons may create some additional ionization upon expulsion from the channel. All of these items would lead to a slower rate of increase in f_e than was calculated, resulting in less charge transport than indicated in the curves of Figure 13. The method that we have used to calculate charge transmission as given in Figure 13 should therefore be considered to yield an upper limit value. Absolute agreement of the calculated and measured charge transport curves would be realized only under ideal conditions (i.e. f_e has no axial dependence, instantaneous ejection of plasma electrons, and no additional ions created by the escaping plasma electrons),

which are not necessarily present in the experiment. However we emphasize that the general trend of our simple calculation and experimental measurement agree.

CHAPTER 6

SUMMARY

In this report we have examined low pressure electron beam propagation in the ion focusing regime where the beam itself was used to create ionization. This work included a parameter study which involved comparison of propagation with different gas species and gas pressures. Injected beam current and transported beam current were measured in order to experimentally determine propagation efficiency. At the lowest pressure tested, 10 mTorr, almost no charge was transported for either helium, nitrogen or argon. As pressure was increased transport improved. Optimum transport occurred for nitrogen and argon at approximately 80 mTorr where 60% of the injected charge was transported a distance of 1 m. For both of these gases at 160 mTorr the transport efficiency dropped, possibly because of secondary electrons created by the escaping plasma electrons. For helium gas, 40% of the charge was transported at 160 mTorr. Because the helium cross section for ionization is relatively small as compared with nitrogen and argon, its optimum pressure for propagation more than likely occurs at a higher pressure than was used in this work.

Several key quantities were measured and include: beam radius, beam transverse temperature, beam voltage, and beam current. These quantities were used to evaluate two conditions necessary for beam propagation. Specifically these conditions are: (1) the beam current must not exceed the space charge limiting current and (2) radial force balance must be achieved. One function not measured which is fundamental in evaluating the propagation conditions was $f_e(t)$. Since the relativistic electron beam was used as the ionizer, the space charge neutralization fraction is time dependent. A simple model which included ionization solely by beam electrons was presented in order to calculate this function. Complete charge neutralization was realized in all cases, the rate at which f_e increased being greater at higher pressure and for gases with higher ionization cross section.

For our particular beam parameters condition (1) was met prior to condition (2) in every case tested. This may be due to the high transverse temperature of our beam. Note that the force balance condition takes into account transverse beam temperature while the limiting current condition does not.

Qualitatively, the charge transport as predicted by the crude model agreed with the experimentally measured transport. While the absolute values of the calculated and measured charge transport are different, the general trends indicated were similar. This is true except at the 160 mTorr pressure for

nitrogen and argon. This may be explained by the observation that here we are approaching the critical pressure necessary to remain in the IFR regime (i.e., 400 mTorr).

Both the model and experiment indicated that propagation is highly dependent on f_e. For low pressures, and gases with small ionization cross sections, ions are produced at a rate such that conditions favorable for propagation are satisfied after much of the beam pulse has already occurred. Here a major part of the beam is used up in creating the ion channel. Conversely, at higher pressures, and with gases with higher ionization cross sections, f_e increases very quickly and propagation conditions may be satisfied very early in the beam pulse, resulting in more efficient propagation.

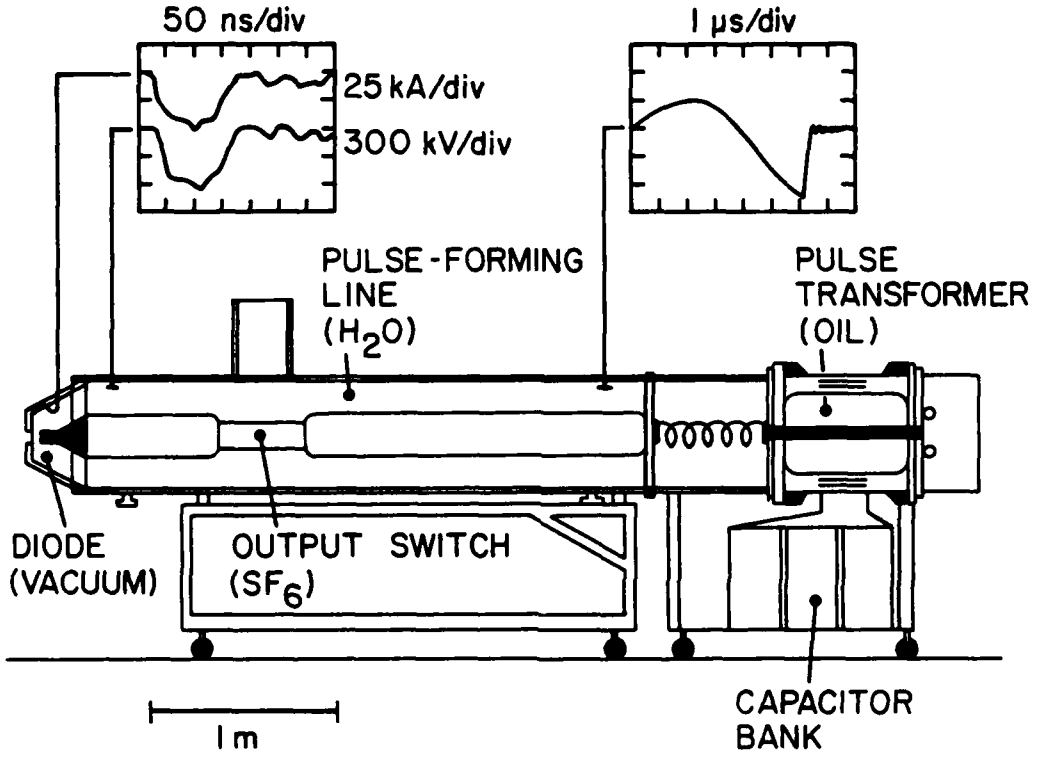

FIGURE 1. TRANSBEAM ACCELERATOR

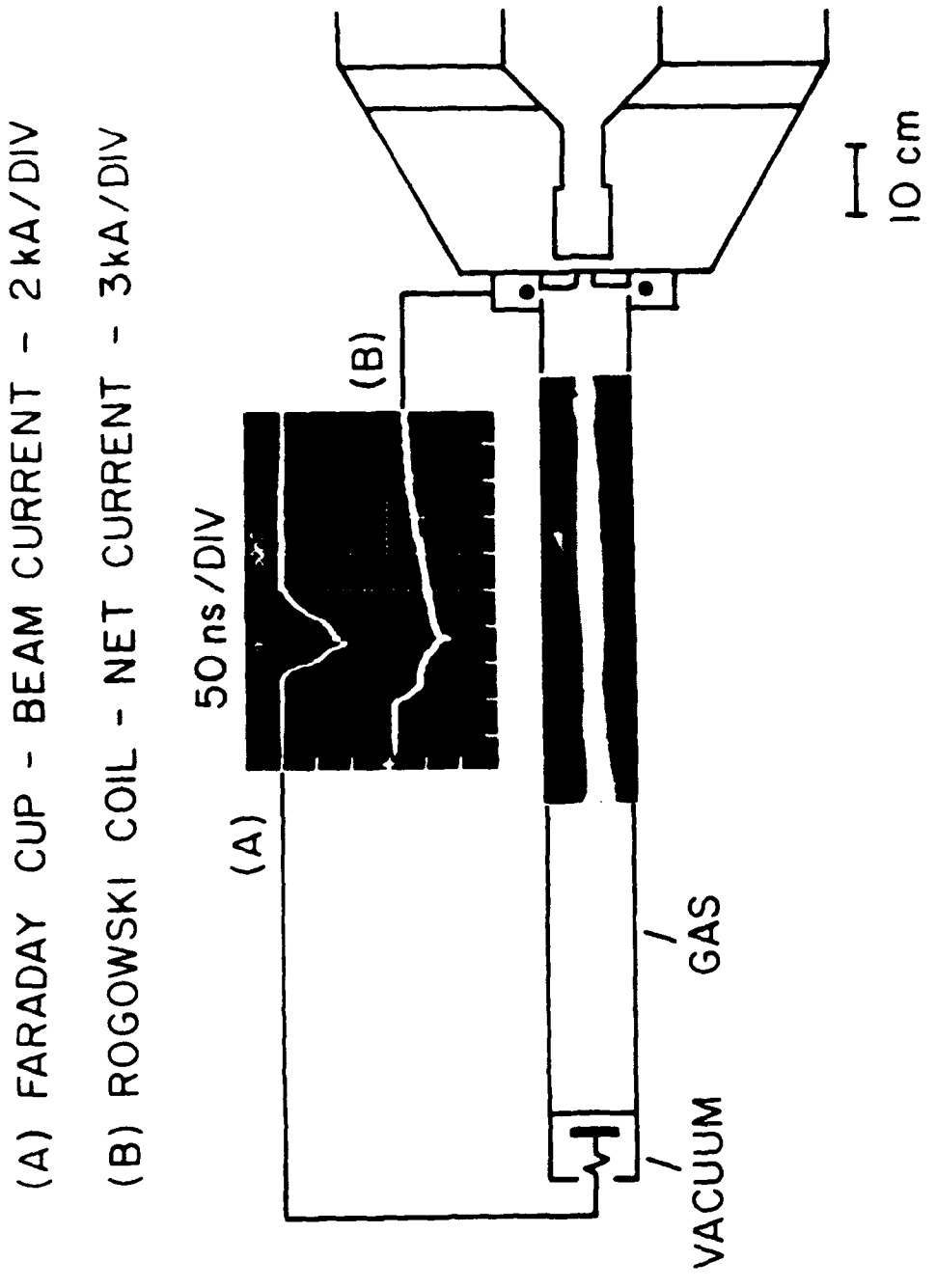

FIGURE 2. EXPERIMENTAL CONFIGURATION

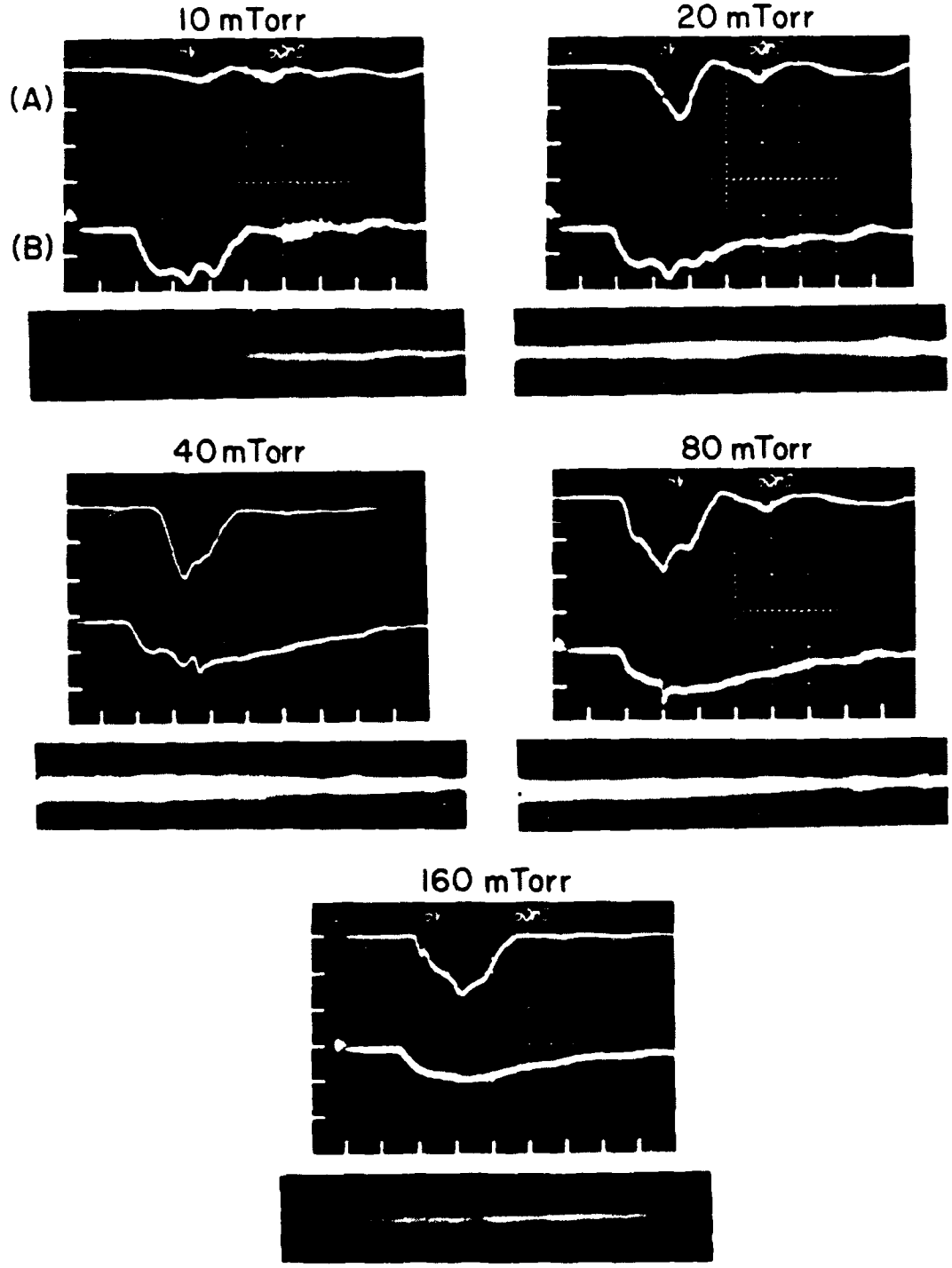

(A) FARADAY CUP - 2 kA/DIV
(B) ROGOWSKI COIL - 3 kA/DIV
HORIZONTAL SCALE - 50 ns/DIV

FIGURE 3. NITROGEN GAS SHOTS

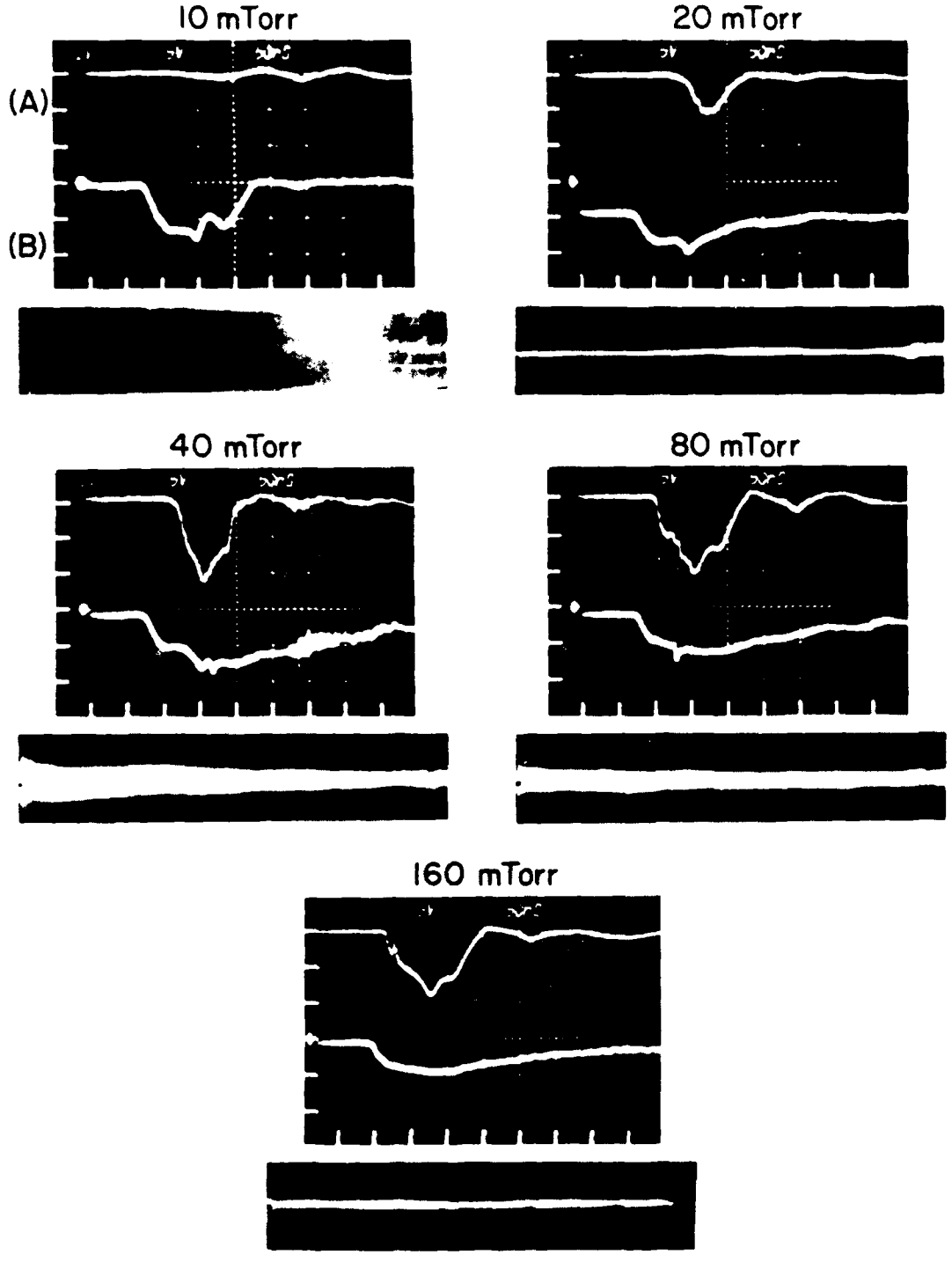

(A) FARADAY CUP - 2 kA/DIV
(B) ROGOWSKI COIL - 3 kA/DIV
HORIZONTAL SCALE - 50 ns/DIV

FIGURE 4. ARGON GAS SHOTS

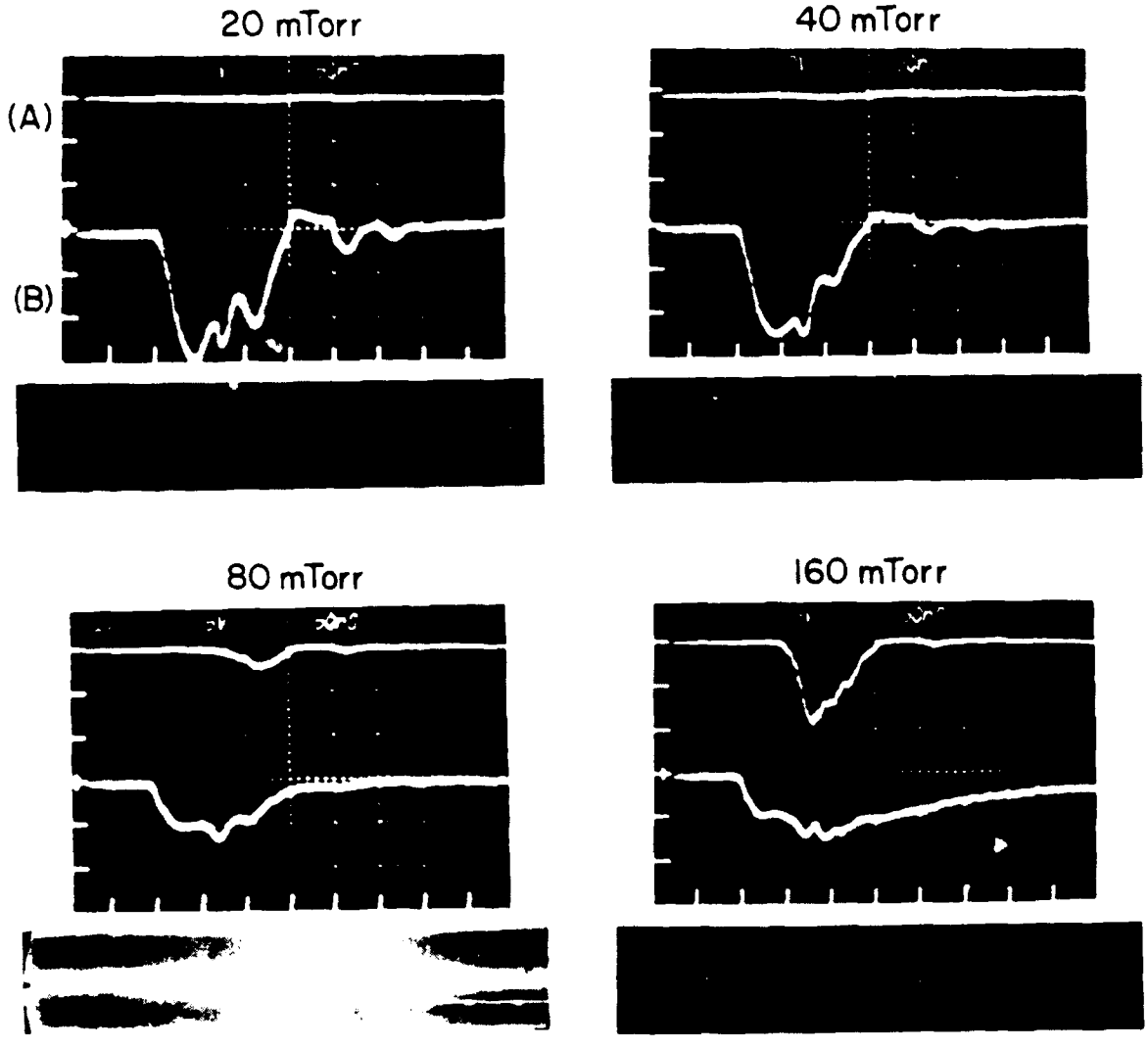

(A) FARADAY CUP - 1 kA/DIV (20, 40 mTorr)
- 2 kA/DIV (80, 160 mTorr)

(B) ROGOWSKI COIL - 1 kA/DIV (20, 40 mTorr)
- 3 kA/DIV (80, 160 mTorr)

HORIZONTAL SCALE - 50 ns/DIV

FIGURE 5. HELIUM GAS SHOTS

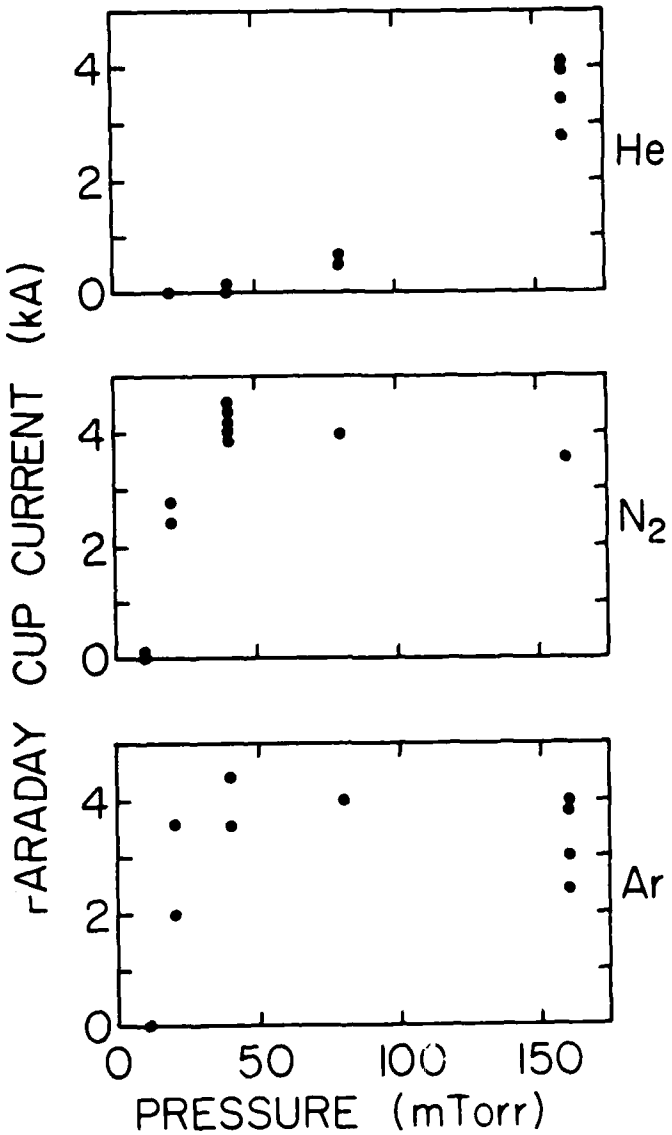

FIGURE 6. FARADAY CUP CURRENT

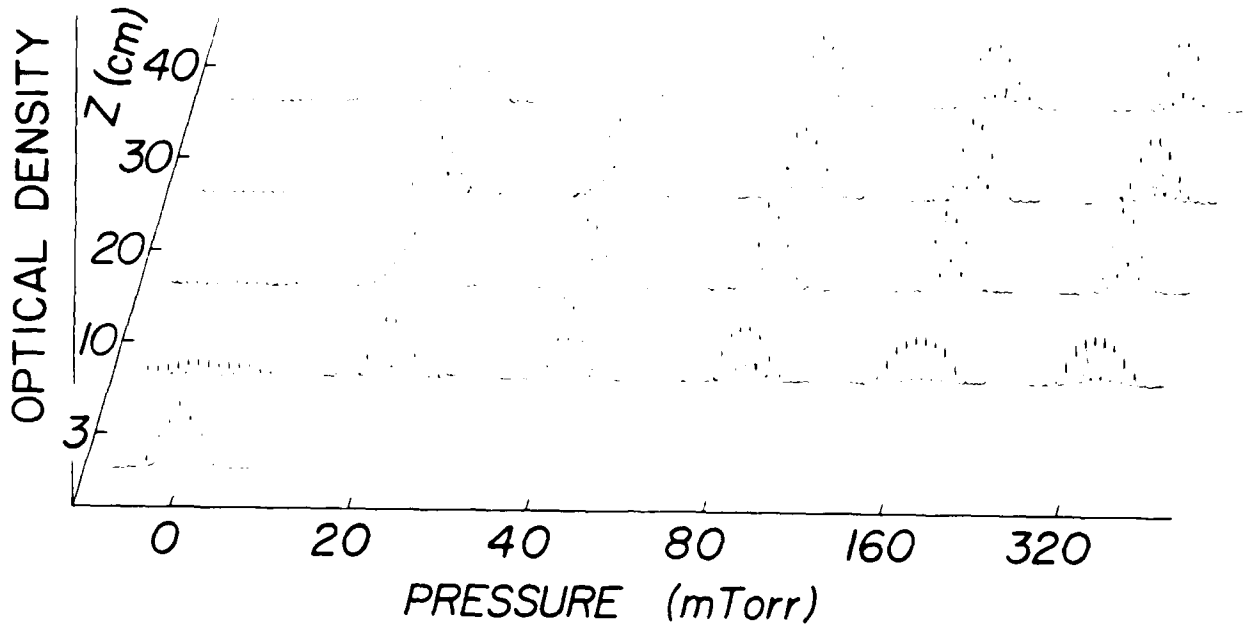

FIGURE 7. MICRODENSITOMETER SCANS, PROPAGATION IN AIR

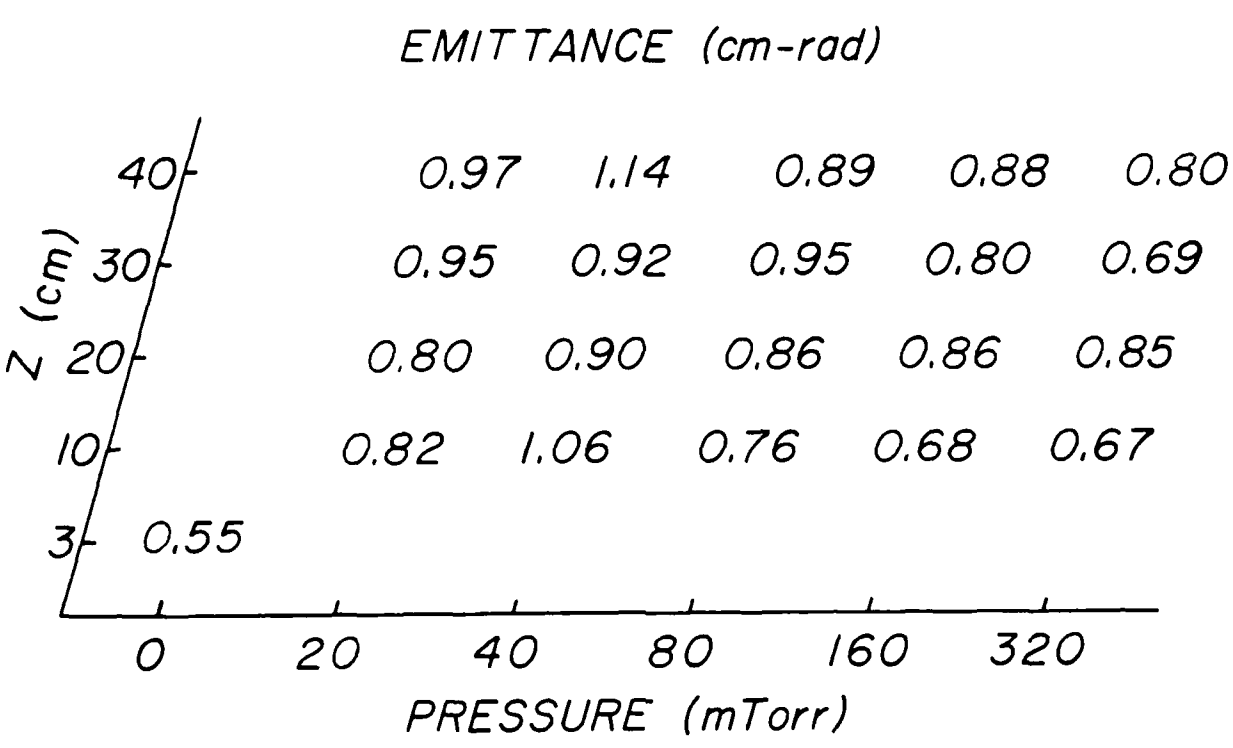

FIGURE 8. RMS EMITTANCE MEASUREMENTS IN AIR

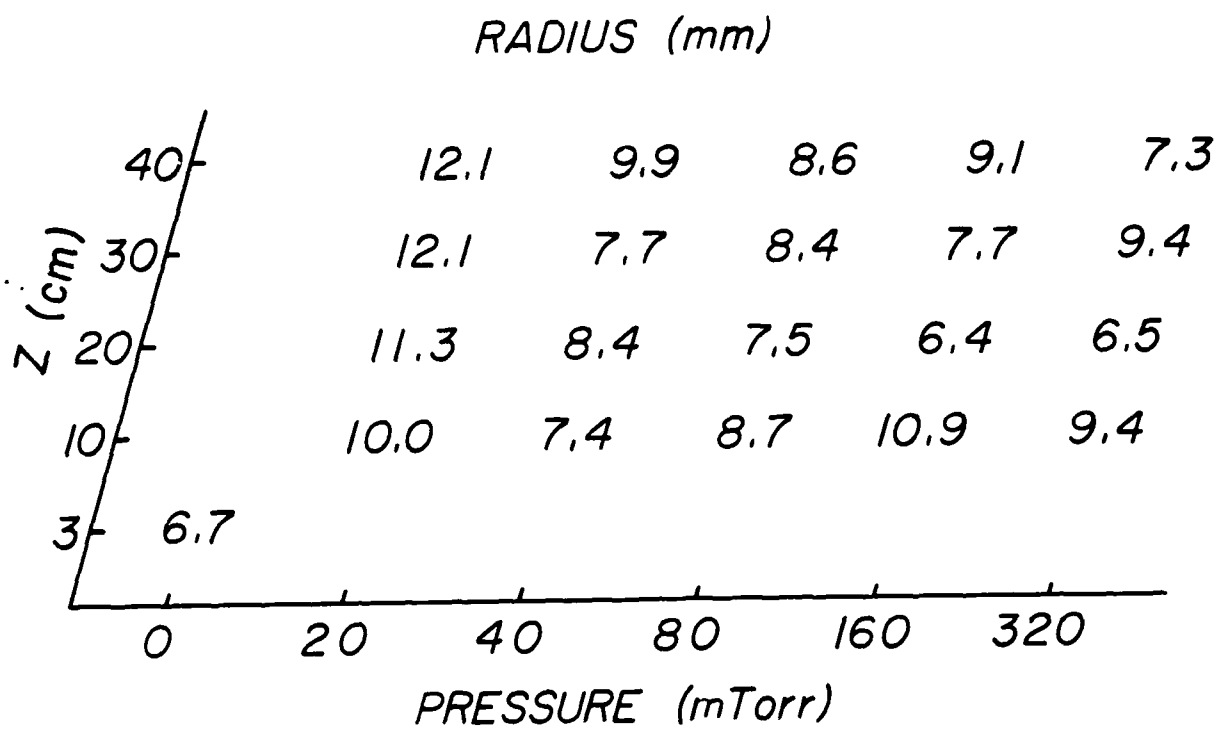

FIGURE 9. RMS RADIUS MEASUREMENTS IN AIR

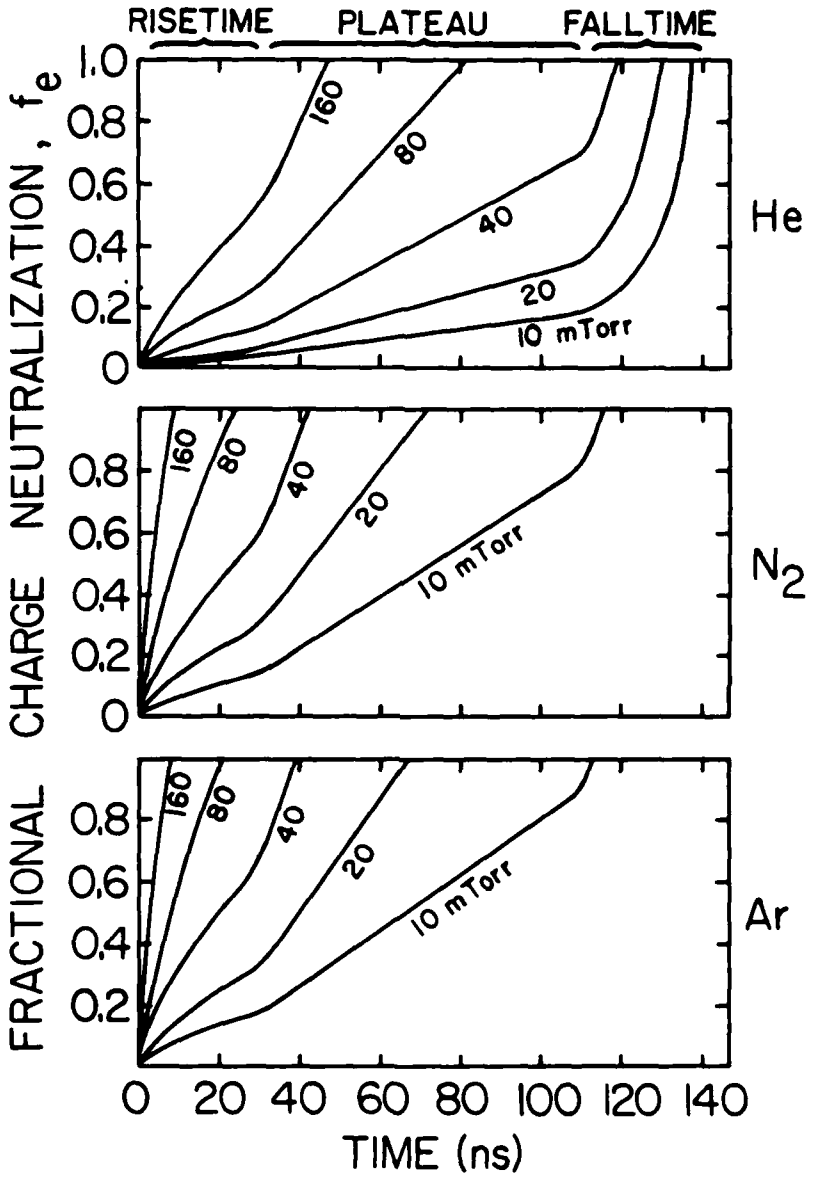

FIGURE 10. CALCULATED SPACE CHARGE NEUTRALIZATION FRACTION

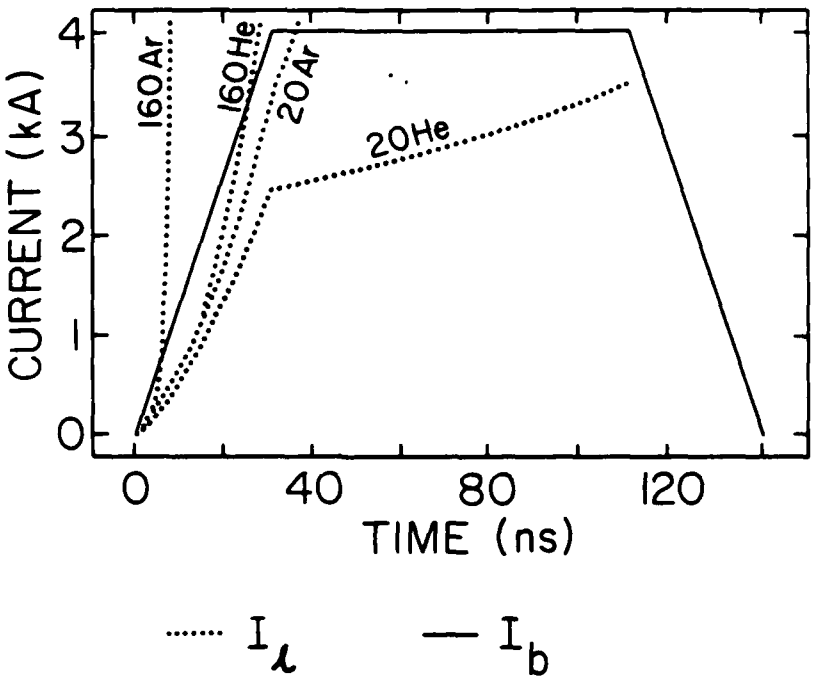

FIGURE 11. COMPARISON OF BEAM CURRENT AND SPACE CHARGE LIMITING CURRENT

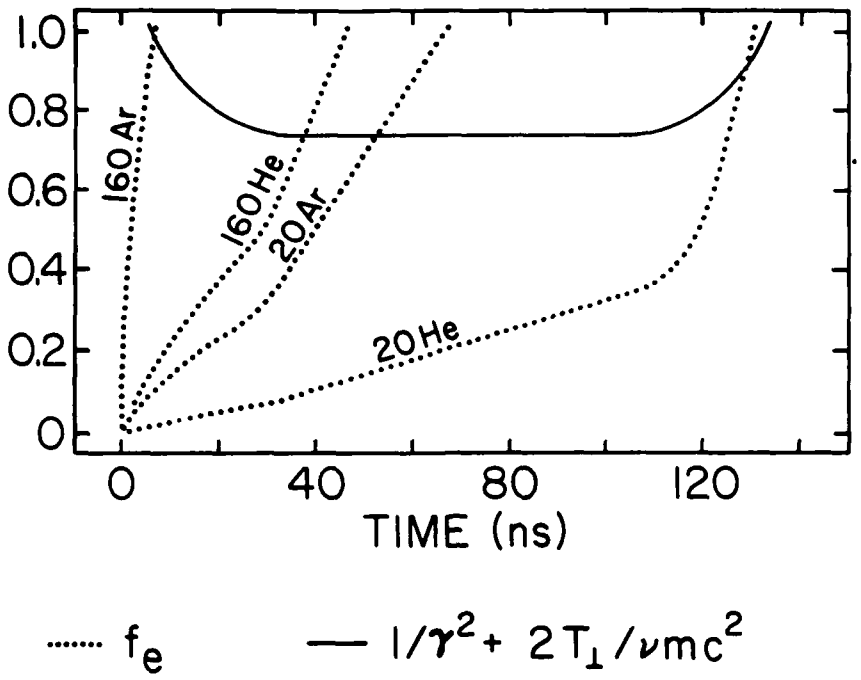

FIGURE 12. COMPARISON OF SPACE CHARGE NEUTRALIZATION FRACTION AND GAMMA-TEMPERATURE TERM

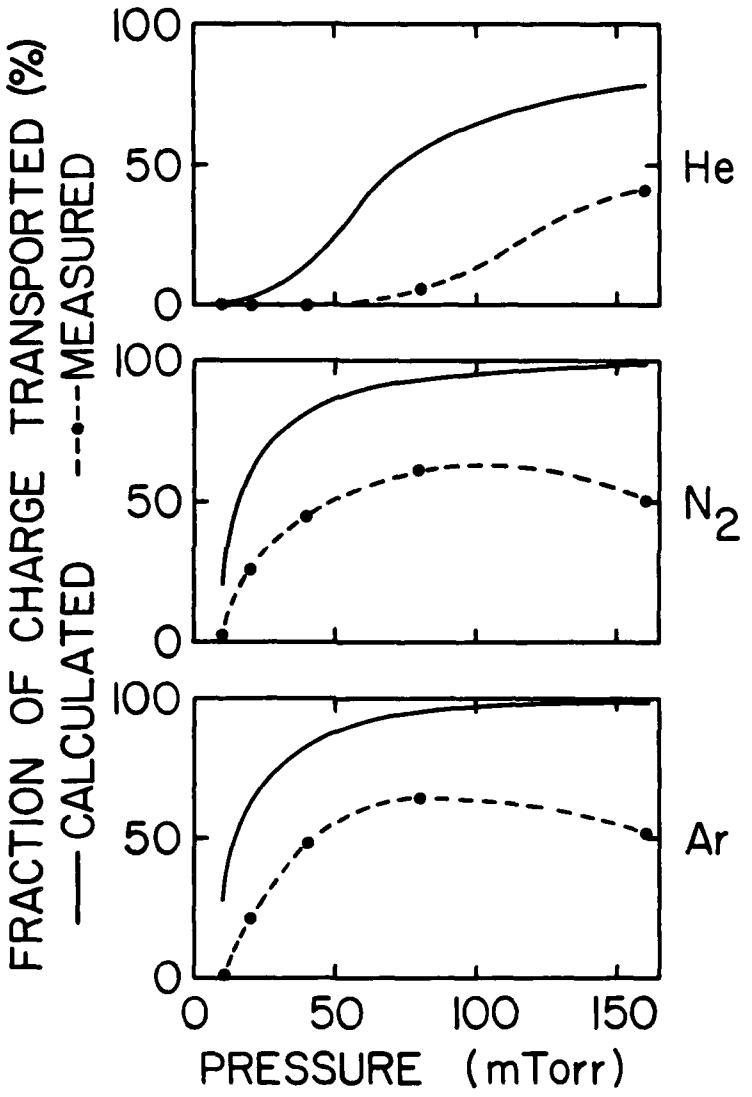

FIGURE 13. COMPARISON OF CALCULATED AND MEASURED CHARGE TRANSPORT EFFICIENCY

TABLE 1. TIME AT WHICH THE BEAM CURRENT FALLS BELOW THE SPACE CHARGE LIMITING CURRENT

Pressure (mTorr)	Time (ns)		
	He	N_2	Ar
10	135	65	61
20	119	39	37
40	73	23	22
80	42	12	11
160	26	6	6

TABLE 2. TIME AT WHICH FORCE EQUILIBRIUM IS REACHED

Pressure (mTorr)	Time (ns)		
	He	N_2	Ar
10	140	101	93
20	130	56	53
40	111	34	33
80	63	18	17
160	37	9	8

REFERENCES

1. Graybill, S. E., "Dynamics of Pulsed High Current Relativistic Electron Beams," IEEE Trans. Nucl. Sci., Vol. 18, No. 3, 1971, p.438.

2. Beal, J. W., Briggs, R. J., and Pearlstein, L. D., "Beam Research Program - Recent Results and Status," Lawrence Livermore National Laboratory report, #UCID-16169, Livermore, CA, 1972.

3. Swain, David W., "Ionization of a Background Gas by a Weak Relativistic Electron Beam," J. Appl. Phys., Vol. 43, No. 2, 1972, p. 396.

4. Miller, P. A., Gerardo, J. B., and Poukey, J. W., "Relativistic Electron Beam Propagation in Low-Pressure Gases," J. Appl. Phys., Vol. 43, No. 7, 1972, p. 3001.

5. Straw, David C., and Miller, R. B., "Dependence of Ion Acceleration on Limiting Current in Relativistic Electron Beams," Appl. Phys. Lett., Vol. 25, No. 7, 1974, p. 379.

6. Miller, Robert B., and Straw, David C., "Observations of Collective Ion Acceleration with Drifting Intense Relativistic Electron Beams," J. Appl. Phys., Vol. 47, No. 5. 1976, p.1897.

7. Fessenden, T. J., Briggs, R. J., Clark, J. C., Lauer, E. J., and Trimble, D. O., "FX-25 Beam Propagation Experiments," Lawrence Livermore National Laboratory report #UCID-17840, Livermore, CA, 1978.

8. Yamagiwa, K., Hopman, H. J., deHaan, P. H., and Janssen, G. C. A. M., "Low Frequency Instability Excited by a Partially Neutralized Relativistic Electron Beam," Plasma Physics, Vol 24, No. 8, 1982, p. 951.

9. Struve, K. W., Lauer, E. J., and Chambers, F. W., "Electron Beam Propagation in the Ion Focused Regime with the Experimental Test Accelerator, "Proceedings of the Fifth International Conference on High-Power Particle Beams," R. J. Briggs and A. J. Toepfer, eds, San Francisco, CA, 1983, p. 408.

10. Bogdankevich, L. S., and Rukhadze, A. A., "Stability of Relativistic Electron Beams in a Plasma and the Problem of Critical Currents," Sov. Phys.-Usp., Vol 14, No. 2., 1971, p. 163.

11. Davidson, R. C., and Uhm, H. S., "Thermal Equilibrium Properties of an Intense Relativistic Electron Beam," Phys. Fluids, Vol.22, No. 7, 1979, p. 1375.

12. Olson, C. L., and Poukey, J. W., "Force-neutral Beams and Limiting Currents," Phys. Rev. A, Vol. 9, No. 6, 1974, p. 2631.

13. Vlasov, M. A., and Nikonov, S. V., "Collisionless Relaxation of a Cold High-Current Electron Beam," Radiotekhnika i elektronika, Vol. 28, No. 5, 1983, p. 131.

14. Briggs R. J., and Yu, S., "Modeling Beam Front Dynamics at Low Gas Pressures," Lawrence Livermore National Laboratory report #UCID-19399, Livermore, CA, 1982.

15. Rohwein, G. J., "A Three Megavolt Transformer for PFL Pulse Charging," IEEE Trans. Nucl. Sci., Vol. 26, No. 3, 1979, p. 4211.

16. Abramyan, E. A., "Transformer Type Accelerators for Intense Electron Beams," IEEE Trans. Nucl. Sci., Vol. 18, No. 3, 1971, p. 447.

17. Humphreys, K. C., and Kantz, A. D., "Radiachromic: A Radiation Monitoring System," Radiat. Phys. Chem., Vol. 9, 1977, p. 737.

18. Namkung, W., and Chojnacki, E. P., "Emittance Measurements of Space-Charge Dominated Electron Beams," Rev. Sci. Instrum., Vol. 57, No. 3, 1986, p. 341.

19. Olson, Craig L., "Charge-Neutralization Processes for Intense Relativistic Electron Beams in Low-Pressure Neutral Gases," Phys. Rev. A, Vol. 11, No. 1, 1975, p. 288.

20. Rieke, F. F., and Prepejchal, W., "Ionization Cross Sections of Gaseous Atoms and Molecules for High-Energy Electrons and Positrons," Phys. Rev. A, Vol. 6, No. 4, 1972, p. 1507.

DISTRIBUTION

	Copies
Strategic Defense Initiative Organization Attn: LTCOL R. L. Gullickson Directed Energy Office The Pentagon Washington, DC 20301-7100	1
Commander Naval Sea Systems Command Attn: Code PMS-405 (CDR W. Bassett) Washington, DC 20362	1
Commander Naval Research Laboratory Attn: Code 4750 (Dr. R. Meger) Code 4751 (Dr. M. Raleigh) Code 4750 (Dr. R. Pechacek) Code 4751 (Dr. D. Murphy)	1 1 1 1
Defense Technical Information Center Cameron Station Alexandria, VA 22314	12
Library of Congress Attn: Gift and Exchange Division Washington, DC 20540	4
Lawrence Livermore National Laboratory Attn. Code L-626 (Dr. F. W. Chambers) Code L-626 (Dr. K. W. Struve) Code L-626 (Dr. E. J. Lauer) Code L-626 (Dr. D. Prono) P. O. Box 808 Livermore, CA 94550	1 1 1 1
Los Alamos National Laboratory Attn: Dr. Joseph Mack Dr. Randolph Carlson Dr. David Moir P. O. Box 1663 Los Alamos, NM 87545	1 1 1
Sandia National Laboratory Attn: Div. 1270 (Dr. R. B. Miller) Div. 1272 (Dr. M. Mazarakis) Div. 1274 (Dr. C. Frost) Div. 1272 (Dr. S. Shope) Div. 1272 (Dr. G. Leifeste) Div. 1272 (Dr. D. Hasti) Div. 1271 (Dr. R. Lipinski) Div. 1241 (Dr. C. Olson) P. O. Box 5800 Albuquerque, NM 87185	1 1 1 1 1 1 1 1
North Carolina State University Attn: Dr. W. O. Doggett Physics Department P. O. Box 8209 Raleigh, NC 27695-8209	1
University of Maryland Attn: Dr. M. J. Rhee Electrical Engineering Department College Park, MD 20742	1
ORI, Inc. Attn: Dr. C. M. Huddleston 1375 Piccard Drive Rockville, MD 20850	1
Pulse Sciences, Inc. Attn: Dr. S. D. Putnam 14796 Wicks Blvd. San Leandro, CA 94577	1

DISTRIBUTION (Cont.)

	Copies
McDonnell Douglas Research Laboratories	
Attn: Dr. J. C. Leader	1
Dr. F. Bieniosek	1
P.O. Box 516	
St. Louis, MO 63166	
Internal Distribution:	
R40	1
R401 (G. Nolting)	1
R41	1
R41 (H. Uhm)	1
R41 (D. Rule)	1
R41 (R. Fiorito)	1
R41 (J. Smith)	40
R41 (R. Chen)	1
R41 (K. Nguyen)	1
R41 (R. Stark)	1
R41 (R. Schneider)	1
R43 (W. Namkung)	1
R43 (J. Choe)	1
E231	9
E232	3

END

3-87

DTIC